

Entanglement Spheres and a UV-IR connection in Effective Field Theories

Natalie Klco^{1,*} and Martin J. Savage^{2,†}

¹*Institute for Quantum Information and Matter (IQIM) and Walter Burke Institute for Theoretical Physics, California Institute of Technology, Pasadena CA 91125*

²*InQubator for Quantum Simulation (IQuS), Department of Physics, University of Washington, Seattle, WA 98195*

(Dated: August 31, 2021 - 1:7)

We show that long-distance quantum correlations probe short-distance physics. Two disjoint regions of the latticized, massless scalar field vacuum are numerically demonstrated to become separable at distances beyond the negativity sphere, which extends to infinity in the continuum limit. The size of this quantum coherent volume is determined by the highest momentum mode supported in the identical regions, each of diameter d . More generally, effective field theories (EFTs), describing a system up to a given momentum scale Λ , are expected to share this feature—entanglement between regions of the vacuum depends upon the UV-completion beyond a separation proportional to Λ . Through calculations extended to three-dimensions, the magnitude of the negativity at which entanglement becomes sensitive to UV physics in an EFT (lattice or otherwise) is conjectured to scale as $\sim e^{-\Lambda d}$, independent of the number of spatial dimensions. It is concluded that two-region vacuum entanglement at increasing separations depends upon the structure of the theory at increasing momentum scales. This phenomenon may be manifest in perturbative QCD processes.

I. INTRODUCTION

Fundamental principles of effective field theories (EFTs) leverage clear separations of energy scales to identify relevant degrees of freedom and to build a systematically improvable hierarchy of local operators. By incorporating all relevant interactions consistent with the symmetries of the theory, this hierarchy accurately captures physics in regimes where scale ratios are small (see, for example, Ref. [1]). While short distance properties require high energy probes (e.g., the exploration of hadronic structure through deep inelastic scattering) or quantum fluctuations (e.g., flavor-changing neutral currents), long distance properties may be informed by infrared (IR) observables at low energies. Thus, long distance physics tends to be insensitive to ultraviolet (UV) modifications incorporated in an EFT through momentum truncations or the “integrating out” of high energy degrees of freedom. In this paper, it is shown that the distillable entanglement between two disjoint regions of a massless scalar field is a long distance observable sensitive to the treatment of the UV degrees of freedom. In particular, a finite momentum truncation, limiting the effective information resolution of the field, will cause distantly separated spatial regions of the field to not only exhibit

vanishing distillable entanglement, but to become separable. As such, momentum-space regularizations in the UV necessarily introduce an IR truncation of the vacuum quantum correlations [2–9] at large spatial distances, limiting the IR regime of EFT validity from the perspective of quantum mechanical inseparability.

Quantum field theory (QFT) has provided a natural unifying perspective of particles as excitations or localized packets of energy embedded in fundamental fields. The many successes calculating entanglement in QFT benefit from an assortment of powerful strategies through lattices, replica tricks, holography, and the AdS/CFT correspondence e.g., [10–29]. Despite these heroic developments, particular parameter regimes e.g., the distillable entanglement between regions distantly separated compared to their size, have evaded analytic control, retaining the importance of numerical explorations.

While the QFT description has been remarkably successful experimentally, conclusions about the underlying structure of nature are limited by the possibility that this success may result from the fact that any relativistic quantum system with Lorentz symmetry and cluster decomposition at long distances will behave as a quantum field at low energies [1, 30]. In fact, considerations in large volumes, inspired by entropy being non-extensive in black hole thermodynamics [31–35], has led to a conjecture that the QFT description egregiously overcounts degrees of freedom [36, 37]. This perspective has inspired the proposal of a relationship between UV and IR trun-

* natklco@caltech.edu

† On leave from the Institute for Nuclear Theory; mjs5@uw.edu

cations in the valid regime of an EFT—limiting the volume to avoid the extensively scaling EFT entropy from exceeding that of a potential black hole [38, 39]. Furthermore, mixing between UV and IR physics has been connected to properties of nonlocality and noncommutative or gravitational generalizations of quantum fields, e.g., [40–46].

This paper demonstrates a connection between UV and IR physics with an observation that the entanglement in the vacuum of a simple quantum field, the massless non-interacting scalar field, is sensitive to high momentum modes at large spatial separations. This extends to mixed states the speculation of Ref. [13], informed by the modewise spatial entanglement structure of harmonic chain bipartite pure states, on the role of short wavelength modes in the persistence of vacuum entanglement. Explicitly, we have extended numerical lattice computations of the logarithmic negativity between pixelated spherical regions to three-dimensions, allowing identification of a dimension-independent scaling of the smallest supported negativity. Such extensions to higher dimension are non-trivial due to cancellations between polynomial and logarithmic-scaling lattice correlation functions generating an exponentially small entanglement, manifesting as a sign problem in the lattice basis. In the process of exploring the entanglement structure of these systems, we have provided numerical evidence, through a separability flow [47], that regions separated beyond the negativity sphere are also separable, precluding the presence of entanglement with positive partial transpose (PPT) in the massless lattice scalar field. The array of calculations presented in this work serve as an explicit example of a more general relationship—long-distance quantum correlations probe short distance physics—broadly affecting the regime of validity for quantum observables in EFTs.

II. VACUUM ENTANGLEMENT SPHERE

As a necessary condition for separability, the negativity [48–51] quantifies the violation of partial transposition—locally negating the momentum in one region for continuous variables [50]—from producing a physical density matrix (non-negative eigenvalues). If a quantum state is separable across a bipartition, partial transposition is a map that preserves the positivity of the density matrix (PPT). Violations to this positivity herald inseparability and thus the presence of entanglement for both mixed and pure quantum states.

Consider the matrix of two-point correlation functions,

$$\hat{G}_{i,j} = \langle \hat{\phi}_i \hat{\phi}_j \rangle \quad , \quad \hat{H}_{i,j} = \langle \hat{\pi}_i \hat{\pi}_j \rangle \quad , \quad (1)$$

where $\{i, j\} \in A \cup B$ for two local field regions A, B . For n_s sites in each region, \hat{G} and \hat{H} are $(2n_s \times 2n_s)$ -dimensional matrices with matrix elements controlled by \mathbf{n} , the vector separating sites $\{i, j\}$. In the thermodynamic limit, the integral representation of the modified Bessel function of the first kind, $I_\nu(z)$, allows a succinct calculation of the necessary correlators as

$$\hat{G}(\mathbf{n}) = \frac{1}{\sqrt{\pi}} \int_0^\infty dx e^{-(m^2+2D)x^2} \prod_i I_{n_i}(2x^2) \quad , \quad (2)$$

and

$$\begin{aligned} \hat{H}(\mathbf{n}) &= (m^2 + 2D)G(\mathbf{n}) - \sum_{\{\mathbf{n}'\}} G(\mathbf{n}') \\ &\rightarrow m^2 G(\mathbf{n}) - \nabla^2 G(\mathbf{n}) \quad , \end{aligned} \quad (3)$$

where $\{\mathbf{n}'\}$ is the set of 2D integer vectors shifted by ± 1 in each direction of the D -dimensional lattice (see Appendix A for further details). The logarithmic negativity is additive

$$\mathcal{N} = - \sum_{i=1}^{2n_s} \log_2 \min(\nu_i^\Gamma, 1) \quad , \quad (4)$$

where ν_i^Γ are the symplectic eigenvalues of the partially transposed covariance matrix, which may be calculated as the eigenvalues of $2\sqrt{\hat{G}\hat{H}^\Gamma}$ [13, 17, 52]. The superscript Γ indicates partial transposition of the conjugate momentum two-point functions and may be implemented, in practice, by negating the matrix element of $\hat{H}_{i,j}$ if the sites at positions $\{i, j\}$ are in different regions $\{A, B\}$ of the field [50].

Numerical evaluations of the negativity between disjoint regions of the massless scalar field have shown that the negativity in the continuum limit with $\tilde{r} \gg d$ decays exponentially as $\mathcal{N} \sim e^{-\beta \frac{\tilde{r}}{d}}$, with \tilde{r} the separation between the field regions and d the diameter of each region. Extractions of the negativity decay constant yield $\beta_{1D} = 2.82(3) \sim 2\sqrt{2}$ [17], $\beta_{2D} = 5.29(4)$ [52], and we currently estimate $\beta_{3D} = 7.6(1)$. Appendix C provides further discussion of this three-dimensional calculation. As proposed in Ref. [52], this progression with dimensionality is consistent with $\beta_D \sim D$, the negativity becoming increasingly localized in higher dimensions. At a finite lattice spacing, where regions experience finite pixelation, there exists a non-perturbative death of negativity

at large separation, $\tilde{r}_{\mathcal{N}}$ [12, 13, 16, 17, 20, 23–26, 28, 29]. The scaling of this negativity sphere with the region pixelation was previously found to be $\tilde{r}_{\mathcal{N}}/d \sim (\gamma/a)d$, with $\gamma_{1D} = 1.114(2)$, $\gamma_{2D} = 0.60(2)$ [52], and we currently estimate $\gamma_{3D} = 0.43(2)$. With a dependence of $\gamma_D \sim D^{-1}$, a more stringent negativity sphere is observed with increasing spatial dimension.

The negativity is not generally a necessary and sufficient condition for determining the separability of Gaussian states. In particular, there is a form of non-distillable entanglement, bound entanglement [53], that may forbid separability while avoiding detection by the negativity criterion [54–59]. By employing the necessary and sufficient Gaussian state separability criterion of Ref. [47], which acts as a flow maintaining the separability (or non-separability) of covariance matrices while systematically simplifying the entanglement structure, it is found that regions of the scalar field outside the negativity sphere are separable. The negativity sphere is thus promoted to an entanglement sphere and describes a finite sized quantum mechanically coherent volume between regions of the field (see Appendix B for further discussion). As such, any observable calculated outside the entanglement sphere will be characterized by factorizable classical probability distributions. For example, the mutual information, which persists outside this entanglement sphere, is there quantifying correlations that are entirely classical.

To the extent that spin models generically are known to exhibit vanishing two-site entanglement beyond a finite site separation [60], the presence of the entanglement sphere is not without precedence. One intriguing implication, however, is that the long distance entanglement known to be present in the continuum quantum field is necessarily captured through the presence of genuine high-body entanglement and a Borromean structure on the lattice—regions entangled at long distances may contain vanishing negativity for all smaller subsets of sites spanning the two regions. This reliance on genuine high-body entanglement at large distances is intuitively consistent with the complexity of low-pixelation regions being insufficient to support long-distance entanglement.

While not exact and currently limited in numerical precision due to the presence of a sign problem exacerbated in higher dimensions, the calculated dependence of the negativity decay and size of the entanglement sphere indicate that the emergence of separability at large distances is set by the UV truncation of the theory. In

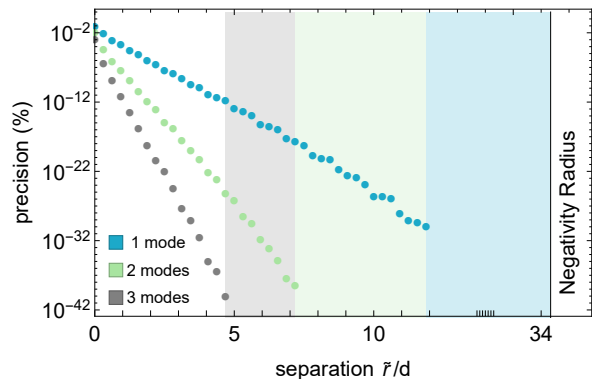


FIG. 1. Precision of the mode-restricted logarithmic negativity as a function of spatial separation in the one-dimensional massless scalar field with region diameter $d = 32$. With increasing separation, the discrepancy vanishes and the entirety of the negativity is captured by the lowest few eigenmodes of $\hat{G}\hat{H}^\Gamma$, indicated by the shaded background.

particular, at the surface of the entanglement sphere, the minimum value of the negativity supported by the field before separability occurs is $\mathcal{N}_{\mathcal{N}} \sim e^{-\beta_D \frac{\tilde{r}_{\mathcal{N}}}{d}} \sim e^{-\beta_D \gamma_D d/a}$. Combining the calculations above to inform the product provides: $\beta_{1D}\gamma_{1D} = 3.14(3)$, $\beta_{2D}\gamma_{2D} = 3.2(1)$, and $\beta_{3D}\gamma_{3D} = 3.2(1)$. The stability of this product with spatial dimension leads us to conjecture that,

$$\mathcal{N}_{\mathcal{N}} \sim e^{-\beta_D \gamma_D d/a} \sim e^{-\frac{\pi d}{a}} \sim e^{-\Lambda d} \quad , \quad (5)$$

where Λ is the scale of the UV truncation, independent of the number of spatial dimensions. For disjoint regions of the vacuum, the threshold negativity below which the field becomes separable is determined by the diameter of each region and the highest allowed momentum mode. In two dimensions, where πd acts as the circumference of the circular field regions, the scaling of the negativity at the entanglement sphere is coincidentally consistent with an area dependence. Though the negativity radius has been conventionally interpreted as a lattice artifact of no consequence to continuum physics, this conjecture indicates that a truncation in the distillable entanglement will be present at long distances in continuum theories with finite UV truncations.

III. ENTANGLEMENT SPHERE AND REGION MOMENTUM

A tangible understanding of the UV-IR connection found in the distillable entanglement at large distances can be elucidated through examination of the dominant

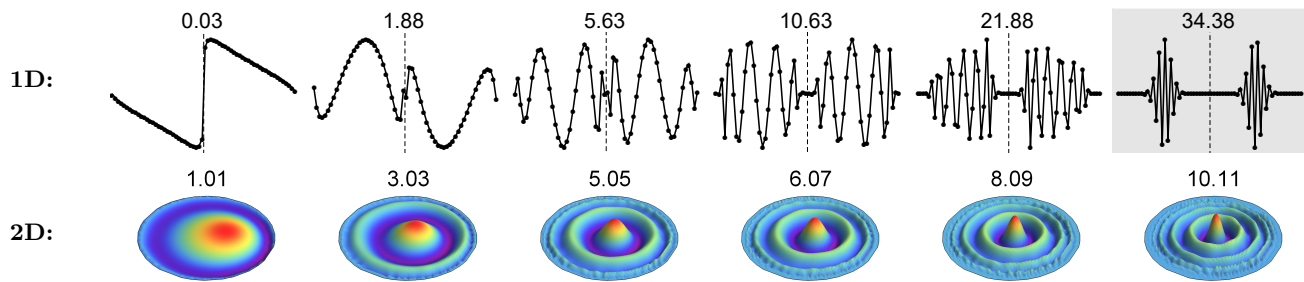


FIG. 2. Negativity ground state wavefunctions of $\hat{G}\hat{H}^\Gamma$ in the massless scalar field in one (top) and two (bottom) spatial dimensions. The 1D wavefunctions are provided across the two regions separated at indicated distances \tilde{r}/d with $d = n_s = 32$ ($\tilde{r}_\mathcal{N}/d = 34.34$). The 2D wavefunctions are shown for one region (negative spatial parity as in 1D) with $d = 64$ for a variety of \tilde{r}/d separations within the entanglement sphere, $\tilde{r}_\mathcal{N}/d \sim 18$.

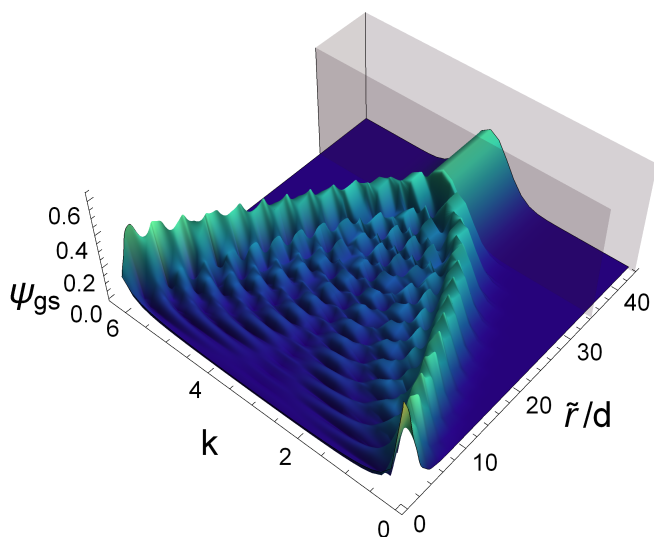


FIG. 3. Momentum space, k , negativity ground state wavefunctions of $\hat{G}\hat{H}^\Gamma$ for the 1D massless scalar field isolated to a single region of $n_s = 32$ as a function of \tilde{r}/d region separation. The gray area at large separation lies outside the negativity radius, $\tilde{r}_\mathcal{N}/d = 34.34$.

$\hat{G}\hat{H}^\Gamma$ right-eigenvector contributing to the logarithmic negativity of Eq. (4). While many symplectic eigenvalues contribute to the negativity at small separations, this number diminishes as the separation increases, as shown in Fig. 1. As the separation approaches the entanglement sphere, the negativity is characterized by the single ground state of $\hat{G}\hat{H}^\Gamma$. In Ref. [52], we examined the negativity ground state wavefunction and found it to evolve to high momentum components with increasing separation. The structure of the $\hat{G}\hat{H}^\Gamma$ ground state within the field regions at increasing separation is shown in Fig. 2 for one and two spatial dimensions. In 1D, the ground

state is demonstrated to have negative parity between the two regions, allowing the depiction of a single region in 2D for visual clarity. At small separations, the negativity ground state is comprised of low-frequency contributions. As the separation grows to multiple region diameters, fluctuations sequentially emerge from the boundary and propagate toward the central peak. These fluctuations are comprised of high-frequency contributions and stress the pixelation of the region. In this long-distance regime, the region negativity ground state wavefunction tends to become rotationally symmetric with a boundary condition vanishing at the edges, allowing the characterization of region entanglement to become effectively one dimensional.

The frequency space representations of the 1D region wavefunctions, $\tilde{\psi}(k) = \frac{1}{\sqrt{n_s}} \sum_x \psi(x) e^{ikx}$, are shown in Fig. 3 for a Brillouin zone $k \in \frac{2\pi}{n_s} \mathbb{Z}_{n_s}$. At small separations, support in momentum space is localized to the regimes of small region momentum at the 0 and 2π boundaries of the Brillouin zone. As the separation between regions increases, the momentum content within the region is driven to the high momentum boundary of $k = \pi$. Outside the entanglement sphere (gray region), the momentum-space wavefunction, now separable, locally saturates the UV truncation and ceases to evolve.

IV. IMPLICATIONS FOR EFFECTIVE FIELD THEORIES

Effective field theories provide a powerful technique for computing low-energy processes in systems with hierarchies in their energy spectrum. The lore is that the predictions of an EFT (valid below some momentum scale Λ) can systematically reproduce those of the full the-

ory (UV-complete) when the IR degrees of freedom and symmetries match. When the full theory is known, local counterterms in the EFT are determined by matching matrix elements computed in both theories. The results of lattice calculations of the negativity discussed in the previous sections indicate that the behaviors of distillable entanglement and separability at long distances of a massless non-interacting scalar field are determined by high-momentum modes of the field, with the radius of the entanglement sphere determined by the UV cutoff. In particular, the exponentially-small negativity between regions of vacuum is lost beyond some dimensionless separation determined by the maximum momentum mode allowed by the lattice spacing, π/a . However, this feature is generic for any low-energy EFT valid up to some momentum scale Λ . The higher the EFT cut off, the larger the separation between regions of the EFT vacuum that remain entangled.

The lattice and other abrupt cutoffs in momentum space lead to a well-defined distance, beyond which regions of the vacuum state are separable. Other regulators can be used to render EFT computations finite by implementing a form factor in momentum or position space e.g., Pauli-Villars (PV) or dimensional regularization (dim. reg.). These provide smooth modifications of perturbative Feynman diagrams, that furnish finite loop diagrams, along with associated counterterms that depend upon the PV mass or the dim. reg. scale, μ . As calculations that can be compared with experiment are independent of the choice of regulator and renormalization scheme, it is the UV-completion of the theory that will determine the behavior (vanishing or otherwise) of negativity at long-distances (see Appendix D). In this way, precision studies of the large-scale entanglement in the quantum vacuum can probe short-distance physics. However, the precise translation of such entanglement studies into constraints on, for instance, beyond the standard model (BSM) physics, remains to be explored.

Rather than an IR constraint on the spatial volume scaling with the inverse UV truncation $L \sim \Lambda^{-3}$ as associated with fundamental bounds on black hole entropy [38, 39], this work identifies a linearly scaling IR truncation, $L \sim \Lambda$, necessary to accurately capture the inseparability of the field ground state. While the core principles of these cutoffs lie in the saturation of spatially localized information, their distinct scaling suggests a stringency crossover—the formation of black holes being the relevant constraint for UV truncations above the

crossover and the separability criterion being the relevant constraint for UV truncations below. To gain some insight into the potential impacts, we provide mass- and length-scales for two different scenarios. Using, in three dimensions, $\tilde{r}_{\mathcal{N}} \sim d^2/(3a) \rightarrow \Lambda d^2/(3\pi)$, and setting $\Lambda = M_{\text{pl}}$ to be the Planck mass, we find that regions of vacuum of a massless noninteracting scalar field approximately the size of the proton are separable at distances beyond ~ 6 km, and that regions approximately the size of an atom are separable beyond $\sim 10^{11}$ km. If the cutoff of the EFT is instead $\Lambda \sim 1$ TeV, then proton sized regions are separable beyond ~ 500 fm and atomic sized regions beyond ~ 5 mm. Evaluating the potential for possible signatures from these distance scales in experiment, one takes pause from the values of negativity at the point of separability, which are $\sim 10^{-1800}$ and $\sim 10^{-2 \times 10^8}$, respectively, for a TeV scale cut off. The magnitude of this effect falls exponentially with separation, imposing what are likely to be severe limits on the constraints that can be determined by experiment.

V. DISCUSSION

By considering massless, non-interacting scalar field theory, the onset of separability between regions of a quantum vacuum in discretized systems has been shown to result from a connection between long-distance and short-distance physics. In particular, the maximum distance between regions of the vacuum that are entangled is directly related to the high-momentum modes of the field. For a lattice field theory, this distance is set by the inverse lattice spacing. While analytic results and a deep understanding of the underlying mechanism(s) remain to be uncovered, numerical explorations indicate that the onset of separability is connected to a saturation of information contained in regions of the pixelated vacuum. This naturally suggests that such effects are present in the vacuum of any quantum field theory that has a UV cutoff, as in the case of any EFT. This violates EFT lore, which assumes that IR physics in a complete theory can be systematically recovered in a low-energy EFT. The present results show, however, that a UV cutoff in an EFT leads to separable regions of the vacuum beyond an entanglement sphere. Further lattice calculations are required to reduce uncertainties associated with the negativity parameters, and to pursue calculations in higher spatial dimensions to better define their dimensional scaling.

For most systems, the discrepancies in measures of entanglement are very small, with estimates suggesting they will be challenging to explore experimentally. However, recent advances in the control of quantum systems capable of representing bosonic fields e.g., [61–64] and the potential to leverage quantum computing technologies as quantum detectors of background field entanglement properties yields numerous directions for potential experimental connection. Beyond the vacuum, experimental signatures of this UV-IR connection, and its implications for low-energy EFTs, may be more profitably sought in excited states of the field theory, in particular, in systems of two or more wavepackets, themselves amenable to detection and measurement. For example, in the EFT description of S-channel scattering of nuclei, entanglement power has been proposed to impact the relevant hierarchy of local operators [46, 65].

While fundamental massless scalar fields do not exist in nature, fields with massless or light excitations and modest or weak interaction strengths e.g., electromagnetism, perturbative QCD, nuclear EFTs around the chiral limit [66, 67], gravity, axions, Bose-Einstein condensates (e.g., Refs. [68, 69]), and neutrinos, may exhibit a modified vacuum entanglement structure at long distances due to UV physics. High energy processes in the nucleon or nucleus, probing distances below the confinement scale with a spatial momentum transfer \mathbf{Q} and UV

cutoff Λ , may be sensitive [70–74] to such modifications for $\tilde{r}_{\mathcal{N}} \gtrsim \Lambda/(3\pi|\mathbf{Q}|^2)$, resulting in a negativity deviation $\sim \exp(-\Lambda/|\mathbf{Q}|)$. Similar signatures are also expected in massive fields, where the long-distance negativity decay becomes Gaussian [17]. It would appear that the phenomenology of entanglement in the quantum vacuum at long distances may depend on what lies beyond the standard model describing electroweak and strong interactions.

ACKNOWLEDGMENTS

We would like to thank Silas Beane, Douglas Beck, Roland Farrell, David Kaplan, Aidan Murran, John Preskill, and Alessandro Roggero for valuable discussions. We have made extensive use of Wolfram Mathematica [75] and the Avapix multiprecision computing toolbox [76] for MATLAB [77]. Numerical results are available upon request. NK is supported in part by the Walter Burke Institute for Theoretical Physics, and by the U.S. Department of Energy Office of Science, Office of Advanced Scientific Computing Research, (DE-SC0020290), and Office of High Energy Physics DE-ACO2-07CH11359. MJS was supported in part by the U.S. Department of Energy, Office of Science, Office of Nuclear Physics, InQubator for Quantum Simulation (IQUS) under Award Number DOE (NP) Award DE-SC0020970.

-
- [1] Steven Weinberg, “Phenomenological Lagrangians,” *Physica A* **96**, 327–340 (1979).
- [2] H. Reeh and S. Schlieder, “Bemerkungen zur unitäräquivalenz von lorentzinvarianten feldern,” *Il Nuovo Cimento (1955-1965)* **22**, 1051–1068 (1961).
- [3] Stephen J Summers and Reinhard Werner, “The vacuum violates bell’s inequalities,” *Physics Letters A* **110**, 257–259 (1985).
- [4] Stephen J Summers and Reinhard Werner, “Bell’s inequalities and quantum field theory. i. general setting,” *Journal of Mathematical Physics* **28**, 2440–2447 (1987), <https://doi.org/10.1063/1.527733>.
- [5] Stephen J Summers and Reinhard Werner, “Bell’s inequalities and quantum field theory. ii. bell’s inequalities are maximally violated in the vacuum,” *Journal of Mathematical Physics* **28**, 2448–2456 (1987), <https://doi.org/10.1063/1.527734>.
- [6] Antony Valentini, “Non-local correlations in quantum electrodynamics,” *Physics Letters A* **153**, 321 – 325 (1991).
- [7] Benni Reznik, “Entanglement from the vacuum,” *Found. Phys.* **33**, 167–176 (2003), arXiv:quant-ph/0212044.
- [8] Benni Reznik, Alex Retzker, and Jonathan Silman, “Violating Bell’s inequalities in the vacuum,” *Phys. Rev. A* **71**, 042104 (2005), arXiv:quant-ph/0310058.
- [9] Edward Witten, “APS Medal for Exceptional Achievement in Research: Invited article on entanglement properties of quantum field theory,” *Rev. Mod. Phys.* **90**, 045003 (2018), arXiv:1803.04993 [hep-th].
- [10] Christoph Holzhey, Finn Larsen, and Frank Wilczek, “Geometric and renormalized entropy in conformal field theory,” *Nucl. Phys. B* **424**, 443–467 (1994), arXiv:hep-th/9403108.
- [11] Curtis G. Callan, Jr. and Frank Wilczek, “On geometric entropy,” *Phys. Lett. B* **333**, 55–61 (1994), arXiv:hep-th/9401072.

- [12] K. Audenaert, J. Eisert, M.B. Plenio, and R.F. Werner, “Entanglement Properties of the Harmonic Chain,” *Phys. Rev. A* **66**, 042327 (2002), arXiv:quant-ph/0205025.
- [13] Alonso Botero and Benni Reznik, “Spatial structures and localization of vacuum entanglement in the linear harmonic chain,” *Phys. Rev. A* **70**, 052329 (2004), arXiv:quant-ph/0403233 [quant-ph].
- [14] Pasquale Calabrese and John L. Cardy, “Entanglement entropy and quantum field theory,” *J. Stat. Mech.* **0406**, P06002 (2004), arXiv:hep-th/0405152.
- [15] Shinsei Ryu and Tadashi Takayanagi, “Holographic derivation of entanglement entropy from AdS/CFT,” *Phys. Rev. Lett.* **96**, 181602 (2006), arXiv:hep-th/0603001.
- [16] Johannes Kofler, Vlatko Vedral, Myungshik S Kim, and Āaslav Brukner, “Entanglement between collective operators in a linear harmonic chain,” *Physical Review A* **73**, 052107 (2006).
- [17] S. Marcovitch, A. Retzker, M.B. Plenio, and B. Reznik, “Critical and noncritical long-range entanglement in Klein-Gordon fields,” *Phys. Rev. A* **80**, 012325 (2009), arXiv:0811.1288 [quant-ph].
- [18] H. Casini and M. Huerta, “Entanglement entropy in free quantum field theory,” *J. Phys. A* **42**, 504007 (2009), arXiv:0905.2562 [hep-th].
- [19] Tatsuma Nishioka, Shinsei Ryu, and Tadashi Takayanagi, “Holographic Entanglement Entropy: An Overview,” *J. Phys. A* **42**, 504008 (2009), arXiv:0905.0932 [hep-th].
- [20] Pasquale Calabrese, John Cardy, and Erik Tonni, “Entanglement entropy of two disjoint intervals in conformal field theory,” *J. Stat. Mech.* **0911**, P11001 (2009), arXiv:0905.2069 [hep-th].
- [21] Pasquale Calabrese and John Cardy, “Entanglement entropy and conformal field theory,” *J. Phys. A* **42**, 504005 (2009), arXiv:0905.4013 [cond-mat.stat-mech].
- [22] Horacio Casini, Marina Huerta, and Robert C. Myers, “Towards a derivation of holographic entanglement entropy,” *JHEP* **05**, 036 (2011), arXiv:1102.0440 [hep-th].
- [23] Pasquale Calabrese, John Cardy, and Erik Tonni, “Entanglement negativity in quantum field theory,” *Phys. Rev. Lett.* **109**, 130502 (2012), arXiv:1206.3092 [cond-mat.stat-mech].
- [24] Pasquale Calabrese, John Cardy, and Erik Tonni, “Entanglement negativity in extended systems: A field theoretical approach,” *J. Stat. Mech.* **1302**, P02008 (2013), arXiv:1210.5359 [cond-mat.stat-mech].
- [25] M. Reza Mohammadi Mozaffar and Ali Mollabashi, “Entanglement in Lifshitz-type Quantum Field Theories,” *JHEP* **07**, 120 (2017), arXiv:1705.00483 [hep-th].
- [26] Andrea Coser, Cristiano De Nobili, and Erik Tonni, “A contour for the entanglement entropies in harmonic lattices,” *Journal of Physics A: Mathematical and Theoretical* **50**, 314001 (2017).
- [27] Paola Ruggiero, Erik Tonni, and Pasquale Calabrese, “Entanglement entropy of two disjoint intervals and the recursion formula for conformal blocks,” *J. Stat. Mech.* **1811**, 113101 (2018), arXiv:1805.05975 [cond-mat.stat-mech].
- [28] Natalie Klco and Martin J. Savage, “Systematically Localizable Operators for Quantum Simulations of Quantum Field Theories,” *Phys. Rev. A* **102**, 012619 (2020), arXiv:1912.03577 [quant-ph].
- [29] Giuseppe Di Giulio and Erik Tonni, “On entanglement hamiltonians of an interval in massless harmonic chains,” *J. Stat. Mech.* **2003**, 033102 (2020), arXiv:1911.07188 [cond-mat.stat-mech].
- [30] Steven Weinberg, “What is quantum field theory, and what did we think it is?” in *Conference on Historical Examination and Philosophical Reflections on the Foundations of Quantum Field Theory* (1996) arXiv:hep-th/9702027.
- [31] Jacob D. Bekenstein, “Black holes and entropy,” *Phys. Rev. D* **7**, 2333–2346 (1973).
- [32] Jacob D. Bekenstein, “Generalized second law of thermodynamics in black hole physics,” *Phys. Rev. D* **9**, 3292–3300 (1974).
- [33] S. W. Hawking, “Black Holes and Thermodynamics,” *Phys. Rev. D* **13**, 191–197 (1976).
- [34] Jacob D. Bekenstein, “A Universal Upper Bound on the Entropy to Energy Ratio for Bounded Systems,” *Phys. Rev. D* **23**, 287 (1981).
- [35] Jacob D. Bekenstein, “Entropy bounds and black hole remnants,” *Phys. Rev. D* **49**, 1912–1921 (1994), arXiv:gr-qc/9307035.
- [36] Gerard 't Hooft, “Dimensional reduction in quantum gravity,” *Conf. Proc. C* **930308**, 284–296 (1993), arXiv:gr-qc/9310026.
- [37] Leonard Susskind, “The World as a hologram,” *J. Math. Phys.* **36**, 6377–6396 (1995), arXiv:hep-th/9409089.
- [38] Andrew G. Cohen, David B. Kaplan, and Ann E. Nelson, “Effective field theory, black holes, and the cosmological constant,” *Phys. Rev. Lett.* **82**, 4971–4974 (1999), arXiv:hep-th/9803132.
- [39] Andrew G. Cohen and David B. Kaplan, “Gravitational contributions to the electron g -factor,” (2021), arXiv:2103.04509 [hep-ph].
- [40] Shiraz Minwalla, Mark Van Raamsdonk, and Nathan Seiberg, “Noncommutative perturbative dynamics,” *JHEP* **02**, 020 (2000), arXiv:hep-th/9912072.
- [41] Alec Matusis, Leonard Susskind, and Nicolaos Toumbas, “The IR / UV connection in the noncommutative gauge theories,” *JHEP* **12**, 002 (2000), arXiv:hep-th/0002075.
- [42] Gregory Minton and Vatche Sahakian, “A New mechanism for non-locality from string theory: UV-IR quantum

- entanglement and its imprints on the CMB,” *Phys. Rev. D* **77**, 026008 (2008), arXiv:0707.3786 [hep-th].
- [43] R. Horvat, A. Ilakovac, J. Trampetic, and J. You, “On UV/IR mixing in noncommutative gauge field theories,” *JHEP* **12**, 081 (2011), arXiv:1109.2485 [hep-th].
- [44] Joanna L. Karczmarek and Charles Rabideau, “Holographic entanglement entropy in nonlocal theories,” *JHEP* **10**, 078 (2013), arXiv:1307.3517 [hep-th].
- [45] Dieter Lust and Eran Palti, “Scalar Fields, Hierarchical UV/IR Mixing and The Weak Gravity Conjecture,” *JHEP* **02**, 040 (2018), arXiv:1709.01790 [hep-th].
- [46] Silas R. Beane and Roland C. Farrell, “Geometry and entanglement in the scattering matrix,” (2020), arXiv:2011.01278 [hep-th].
- [47] G. Giedke, B. Kraus, M. Lewenstein, and J. I. Cirac, “Entanglement criteria for all bipartite gaussian states,” *Phys. Rev. Lett.* **87**, 167904 (2001).
- [48] Michal Horodecki, Pawel Horodecki, and Ryszard Horodecki, “On the necessary and sufficient conditions for separability of mixed quantum states,” *Phys. Lett. A* **223**, 1 (1996), arXiv:quant-ph/9605038.
- [49] G. Vidal and R.F. Werner, “Computable measure of entanglement,” *Phys. Rev. A* **65**, 032314 (2002), arXiv:quant-ph/0102117.
- [50] R. Simon, “Peres-Horodecki Separability Criterion for Continuous Variable Systems,” *Phys. Rev. Lett.* **84**, 2726–2729 (2000), arXiv:quant-ph/9909044.
- [51] M. B. Plenio, “Logarithmic Negativity: A Full Entanglement Monotone That is not Convex,” *Phys. Rev. Lett.* **95**, 090503 (2005), arXiv:quant-ph/0505071.
- [52] Natalie Klco and Martin J. Savage, “Geometric Quantum Information Structure in Quantum Fields and their Lattice Simulation,” *Phys. Rev. D* **103**, 065007 (2021), arXiv:2008.03647 [quant-ph].
- [53] Michał Horodecki, Paweł Horodecki, and Ryszard Horodecki, “Mixed-state entanglement and distillation: Is there a “bound” entanglement in nature?” *Phys. Rev. Lett.* **80**, 5239–5242 (1998).
- [54] Charles H. Bennett, David P. DiVincenzo, Tal Mor, Peter W. Shor, John A. Smolin, and Barbara M. Terhal, “Unextendible Product Bases and Bound Entanglement,” *Phys. Rev. Lett.* **82**, 5385–5388 (1999), arXiv:quant-ph/9808030 [quant-ph].
- [55] Dagmar Bruß and Asher Peres, “Construction of quantum states with bound entanglement,” *Phys. Rev. A* **61**, 030301 (2000), arXiv:quant-ph/9911056 [quant-ph].
- [56] Paweł Horodecki and Maciej Lewenstein, “Bound entanglement and continuous variables,” *Phys. Rev. Lett.* **85**, 2657–2660 (2000).
- [57] R. F. Werner and M. M. Wolf, “Bound Entangled Gaussian States,” *Phys. Rev. Lett.* **86**, 3658–3661 (2001), arXiv:quant-ph/0009118 [quant-ph].
- [58] John A. Smolin, “Four-party unlockable bound entangled state,” *Phys. Rev. A* **63**, 032306 (2001), arXiv:quant-ph/0001001 [quant-ph].
- [59] Heinz-Peter Breuer, “Optimal Entanglement Criterion for Mixed Quantum States,” *Phys. Rev. Lett.* **97**, 080501 (2006), arXiv:quant-ph/0605036 [quant-ph].
- [60] K. M. R Audenaert, J. Eisert, and M. B. Plenio, “Entanglement in systems of interacting harmonic oscillators,” in *Quantum information with continuous variables of atoms and light*, edited by N. J. Cerf, G. Leuchs, and E. S. Polzik (Imperial College Press, London, 2007) pp. 43–62.
- [61] Hui Wang, M. P. Blencowe, C. M. Wilson, and A. J. Rimberg, “Mechanically generating entangled photons from the vacuum: A microwave circuit-acoustic resonator analog of the oscillatory Unruh effect,” *Phys. Rev. A* **99**, 053833 (2019), arXiv:1811.10065 [quant-ph].
- [62] Eric T. Holland, Kyle A. Wendt, Konstantinos Kravvaris, Xian Wu, W. Erich Ormand, Jonathan L DuBois, Sofia Quaglioni, and Francesco Pederiva, “Optimal Control for the Quantum Simulation of Nuclear Dynamics,” *Phys. Rev. A* **101**, 062307 (2020), arXiv:1908.08222 [quant-ph].
- [63] Ananda Roy, Dirk Schuricht, Johannes Hauschild, Frank Pollmann, and Hubert Saleur, “The quantum sine-Gordon model with quantum circuits,” (2020), arXiv:2007.06874 [quant-ph].
- [64] Jimmy S. C. Hung, J. H. Busnaina, C. W. Sandbo Chang, A. M. Vadiraj, I. Nsanzineza, E. Solano, H. Alaieian, E. Rico, and C. M. Wilson, “Quantum simulation of the bosonic creutz ladder with a parametric cavity,” (2021), arXiv:2101.03926 [quant-ph].
- [65] Silas R. Beane, David B. Kaplan, Natalie Klco, and Martin J. Savage, “Entanglement Suppression and Emergent Symmetries of Strong Interactions,” *Phys. Rev. Lett.* **122**, 102001 (2019), arXiv:1812.03138 [nucl-th].
- [66] Sean Fleming, Thomas Mehen, and Iain W. Stewart, “NNLO corrections to nucleon-nucleon scattering and perturbative pions,” *Nucl. Phys. A* **677**, 313–366 (2000), arXiv:nucl-th/9911001.
- [67] S. R. Beane, Paulo F. Bedaque, M. J. Savage, and U. van Kolck, “Towards a perturbative theory of nuclear forces,” *Nucl. Phys. A* **700**, 377–402 (2002), arXiv:nucl-th/0104030.
- [68] Philipp Kunkel, Maximilian Prüfer, Helmut Strobel, Daniel Linnemann, Anika Frölian, Thomas Gasenzer, Martin Gärttner, and Markus K. Oberthaler, “Spatially distributed multipartite entanglement enables EPR steering of atomic clouds,” *Science* **360**, 413–416 (2018), arXiv:1708.02407 [cond-mat.quant-gas].
- [69] N. Sánchez-Kuntz and S. Förlinger, “Spatial entanglement in interacting Bose-Einstein condensates,” (2020), arXiv:2011.11076 [cond-mat.quant-gas].
- [70] Dmitri E. Kharzeev and Eugene M. Levin, “Deep inelastic scattering as a probe of entanglement,” *Phys. Rev. D*

- 95**, 114008 (2017), arXiv:1702.03489 [hep-ph].
- [71] O. K. Baker and D. E. Kharzeev, “Thermal radiation and entanglement in proton-proton collisions at energies available at the CERN Large Hadron Collider,” *Phys. Rev. D* **98**, 054007 (2018), arXiv:1712.04558 [hep-ph].
- [72] Jürgen Berges, Stefan Floerchinger, and Raju Venugopalan, “Entanglement and thermalization,” *Nucl. Phys. A* **982**, 819–822 (2019), arXiv:1812.08120 [hep-th].
- [73] Zhoudunming Tu, Dmitri E. Kharzeev, and Thomas Ullrich, “Einstein-Podolsky-Rosen Paradox and Quantum Entanglement at Subnucleonic Scales,” *Phys. Rev. Lett.* **124**, 062001 (2020), arXiv:1904.11974 [hep-ph].
- [74] Dmitri E. Kharzeev and Eugene Levin, “Deep inelastic scattering as a probe of entanglement: confronting experimental data,” (2021), arXiv:2102.09773 [hep-ph].
- [75] Wolfram Research, Inc., “Mathematica, Version 11.1,” Champaign, IL, 2020.
- [76] Advanpix LLC., “Multiprecision computing toolbox for matlab,” .
- [77] MATLAB, *version 9.8.0.1396136 (R2020a) Update 3* (The MathWorks Inc., Natick, Massachusetts, 2020).
- [78] DLMF, “*NIST Digital Library of Mathematical Functions*,” <http://dlmf.nist.gov/>, Release 1.0.28 of 2020-09-15, f. W. J. Olver, A. B. Olde Daalhuis, D. W. Lozier, B. I. Schneider, R. F. Boisvert, C. W. Clark, B. R. Miller, B. V. Saunders, H. S. Cohl, and M. A. McClain, eds.
- [79] Geza Giedke, L-M Duan, J Ignacio Cirac, and Peter Zoller, “Distillability criterion for all bipartite gaussian states,” *Quantum Information and Computation* **1**, 79–86 (2001), arXiv:quant-ph/0104072 [quant-ph].

Appendix A: Lattice Correlation Functions in the Thermodynamic Limit

For free scalar fields, two-point correlation functions define the information content in the field. In this appendix, formulations of these expectation values are presented in the thermodynamic limit of large lattices with a form conducive to computation. In 1D and 2D, analytic expressions are provided, while in higher dimensions, a one dimensional integral is provided with convergence that improves with increasing dimension. For $D \geq 2$, correlation functions are IR convergent, allowing the mass to be reliably set to zero.

For arbitrary D , the two-point lattice field correlation function with unit lattice spacing and field separation described by a vector of positive integers, \mathbf{n} , is

$$\langle \phi(0)\phi(\mathbf{n}) \rangle = G(\mathbf{n}) = \sum_p \frac{e^{i\mathbf{p}\cdot\mathbf{n}}}{2L^D} \frac{1}{\sqrt{m^2 + 4 \sum_i \sin^2\left(\frac{p_i}{2}\right)}}, \quad (\text{A1})$$

for $p_i \in \frac{2\pi}{L}\mathbb{Z}_L$ with \mathbb{Z}_L the set of integers between 0 and $(L-1)$. In the thermodynamic limit ($L \rightarrow \infty$),

$$G(\mathbf{n}) = \frac{1}{2\pi^D} \int_0^\pi d^D p \frac{\prod_i \cos(p_i n_i)}{\sqrt{m^2 + 4 \sum_i \sin^2\left(\frac{p_i}{2}\right)}}, \quad (\text{A2})$$

with $d^d p = \prod_i dp_i$. A Gaussian integral may be introduced to capture the radical in the denominator

$$G(\mathbf{n}) = \frac{1}{2\pi^D} \int_0^\pi d^D p \prod_i \cos(p_i n_i) \left[\frac{2}{\sqrt{\pi}} \int_0^\infty dx e^{-(m^2+2D)x^2} e^{\sum_i (2 \cos p_i)x^2} \right]. \quad (\text{A3})$$

The integral representation of the modified Bessel function of the first kind may subsequently be identified to yield,

$$G(\mathbf{n}) = \frac{1}{\sqrt{\pi}} \int_0^\infty dx e^{-(m^2+2D)x^2} \prod_i I_{n_i}(2x^2), \quad (\text{A4})$$

where, for integer order, the modified Bessel function may be expressed as,

$$I_\alpha(z) = \frac{1}{\pi} \int_0^\pi d\theta e^{z \cos \theta} \cos \alpha \theta. \quad (\text{A5})$$

The resulting expression for the two-point correlation function is a single integral for any D . As $I_\alpha(z) \sim e^z/\sqrt{2\pi z}$ for large arguments, the convergence of these integrals improves with increasing D .

Employing similar procedures for the two-point functions of conjugate momentum field operators yields analogous computationally advantageous expressions. In the thermodynamic limit with massless fields, the expectation value may be written as,

$$\langle \pi(0)\pi(\mathbf{n}) \rangle \equiv H(\mathbf{n}) \quad (\text{A6})$$

$$= \frac{1}{2\pi^D} \int_0^\pi d^D p \prod_i \cos(p_i n_i) \sqrt{m^2 + 4 \sum_i \sin^2 \left(\frac{p_i}{2} \right)} \quad (\text{A7})$$

$$= \frac{1}{2\pi^D} \int_0^\pi d^D p \frac{\prod_i \cos(p_i n_i)}{\sqrt{m^2 + 4 \sum_i \sin^2 \left(\frac{p_i}{2} \right)}} \left(m^2 + 2D - 2 \sum_j \cos(p_j) \right) . \quad (\text{A8})$$

Associating the additional $\cos(p_i)$ factors with a partial derivative of the modified Bessel function, Eq. (A5), with respect to its argument, the correlator becomes

$$H(\mathbf{n}) = \int_0^\infty \frac{e^{-(m^2+2D)x^2}}{\sqrt{\pi}} \left((m^2 + 2D) \prod_i I_{n_i}(2x^2) - 2 \sum_j \frac{\partial_j}{\partial(2x^2)} \prod_i I_{n_i}(2x^2) \right) , \quad (\text{A9})$$

where $\frac{\partial_j}{\partial(2x^2)}$ indicates the argument derivative of the Bessel function associated with the j^{th} lattice direction. Given that this is expressible as the average of the Bessel functions of neighboring order,

$$\partial_z I_\alpha(z) = \frac{I_{\alpha-1}(z) + I_{\alpha+1}(z)}{2} , \quad (\text{A10})$$

$H(\mathbf{n})$ can be written as a linear combination of field correlators,

$$\begin{aligned} H(\mathbf{n}) &= (m^2 + 2D)G(\mathbf{n}) - \sum_{\{\mathbf{n}'\}} G(\mathbf{n}') , \\ &\rightarrow m^2 G(\mathbf{n}) - \nabla^2 G(\mathbf{n}) , \end{aligned} \quad (\text{A11})$$

where the set $\{\mathbf{n}'\}$ is the set of 2D integer vectors shifted by ± 1 in each possible direction of the D dimensional lattice. Thus, the numerical stability of the field correlators extends to correlators in conjugate momentum space.

1. One Spatial Dimension

The integral expression of Eq. (2) in 1D can be evaluated in closed form as,

$$G(n) = \frac{1}{2\sqrt{\pi}(2+m^2)^{n+1/2}} \Gamma\left[\frac{1}{2} + n\right] {}_2\tilde{F}_1\left(\frac{1+2n}{4}, \frac{3+2n}{4}; \frac{4}{(2+m^2)^2}\right) , \quad (\text{A12})$$

where ${}_2\tilde{F}_1\left(\frac{a,b}{c}; z\right) = {}_2F_1\left(\frac{a,b}{c}; z\right) / \Gamma(c)$ is the regularized hypergeometric function, consistent with e.g., Ref. [26].

The ${}_2F_1$ function is finite for finite values of its parametric arguments and for $|z| < 1$. Thus, the mass in 1D is a necessary IR regulator that must be maintained nonzero throughout calculations.

2. Two Spatial Dimensions

In 2D, the field correlators can be solved analytically, a valuable capability for the finely-pixelated wavefunctions presented in Fig. 2 of the main text. Using the following identity for the product of two modified Bessel functions of equal argument [78, Eq. 10.31.3], the two point function of Eq. (2) becomes,

$$G(n_x, n_y) = \frac{1}{\sqrt{\pi}} \int_0^\infty dx e^{-(m^2+4)x^2} x^{2(n_x+n_y)} \sum_{k=0}^\infty \frac{(n_x + n_y + k + 1)_k x^{4k}}{k! \Gamma(n_x + k + 1) \Gamma(n_y + k + 1)} , \quad (\text{A13})$$

relying on the closure of a product of ${}_0F_1$ functions into a ${}_2F_3$ generalized hypergeometric function. The x integral is calculated as a Gaussian moment,

$$G(n_x, n_y) = \frac{1}{2(4+m^2)^{\frac{1+2n_x+2n_y}{2}} \sqrt{\pi}} \sum_{k=0}^{\infty} \frac{(n_x+n_y+k+1)_k}{k! \Gamma(n_x+k+1) \Gamma(n_y+k+1)} \frac{\Gamma(\frac{1}{2}+2k+n_x+n_y)}{(4+m^2)^{2k}}. \quad (\text{A14})$$

Using the Legendre duplication relation of the Gamma function and the associated Pochhammer identity,

$$\left(\frac{z}{2}\right)_n \left(\frac{z}{2} + \frac{1}{2}\right)_n = 2^{-2n} (z)_{2n}, \quad \frac{\left(\frac{a+b+1}{2}\right)_k \left(\frac{a+b+2}{2}\right)_k}{(a+b+1)_k} = 4^{-k} (1+a+b+k)_k, \quad (\text{A15})$$

a generalized hypergeometric function can be identified for the two-point correlation function,

$$G(n_x, n_y) = \frac{1}{2\sqrt{\pi}(4+m^2)^{1/2+n_x+n_y}} \frac{\Gamma(\frac{1}{2}+n_x+n_y)}{\Gamma(n_x+1)\Gamma(n_y+1)} \times {}_4F_3 \left(\begin{matrix} \frac{n_x+n_y+1}{2}, \frac{n_x+n_y+2}{2}, \frac{n_x+n_y}{2} + \frac{1}{4}, \frac{n_x+n_y}{2} + \frac{3}{4} \\ 1+n_x, 1+n_y, 1+n_x+n_y \end{matrix}; \frac{16}{(4+m^2)^2} \right), \quad (\text{A16})$$

where

$${}_pF_q \left(\begin{matrix} a_1, \dots, a_p \\ b_1, \dots, b_q \end{matrix}; z \right) \equiv \sum_{k=0}^{\infty} \frac{z^k}{k!} \frac{\prod_{j=1}^p (a_j)_k}{\prod_{\ell=1}^q (b_\ell)_k}. \quad (\text{A17})$$

In the massless limit, the argument of the hypergeometric function becomes unity. Because the $|z|=1$ case is finite and well defined for ${}_4F_3 \left(\begin{matrix} a_1, a_2, a_3, a_4 \\ b_1, b_2, b_3 \end{matrix}; z \right)$ if $\sum_j b_j - \sum_j a_j > 0$ (which will always be satisfied above), the mass does not need to be retained as an explicit IR regulator. The correlators of conjugate momentum operators are related through Eq. (3) as,

$$H(n_x, n_y) = (4+m^2)G(n_x, n_y) - G(n_x-1, n_y) - G(n_x+1, n_y) - G(n_x, n_y-1) - G(n_x, n_y+1). \quad (\text{A18})$$

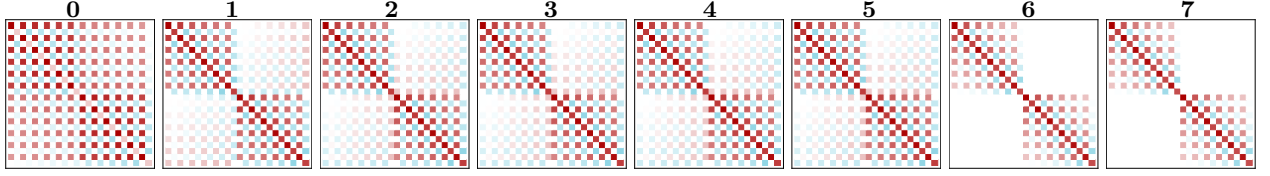
It is expected that analytic expressions exist for the field correlators in higher dimension, $D > 2$, though their form remains elusive. For 3D, it has been computationally practical (leveraging the mentioned improving convergence in higher dimensions) to calculate the lattice two-point functions numerically through a truncated expansion of modified Bessel functions in Eq. (2).

Appendix B: Logarithmic Negativity, Gaussian Separability Criteria and the Entanglement Sphere

While logarithmic negativity can be difficult to interpret as an entanglement measure in general, its current application, combined with the separability criterion of Ref. [47] and the distillation criterion of Ref. [79], has yielded a uniquely informative quantification of quantum correlations in the free lattice scalar field theory vacuum. Generically, negativity has been connected to the operational measure of *distillable entanglement* i.e., the population of entangled pairs that can be asymptotically extracted from an ensemble of the state through local interactions [49]. Thus, the negativity will inform the spacelike entanglement that could be extracted by locally interacting detectors.

As an upper bound to the distillable entanglement, a vanishing logarithmic negativity between regions of a field indicates that two sensors/detectors interacting at spacelike separations with the field would never themselves become entangled, even if the local regions of the field are expressed with a single non-separable quantum wavefunction. The latter extension indicates that a vanishing negativity is generically inconclusive with respect to the separability of the regions (e.g., due to the possibility of bound entanglement [53]). Non-zero negativity, however, is conclusive with respect to inseparability. Because negativity quantifies the physical validity of a density matrix after transformation by a particular local positive map (partial transposition), any violation of physicality heralds the presence of entanglement. However, as an upper bound, a non-zero negativity generically carries no conclusive information about the operational entanglement structure of the field.

flow step:



conclusion:

? ? ? ? ? sep sep sep

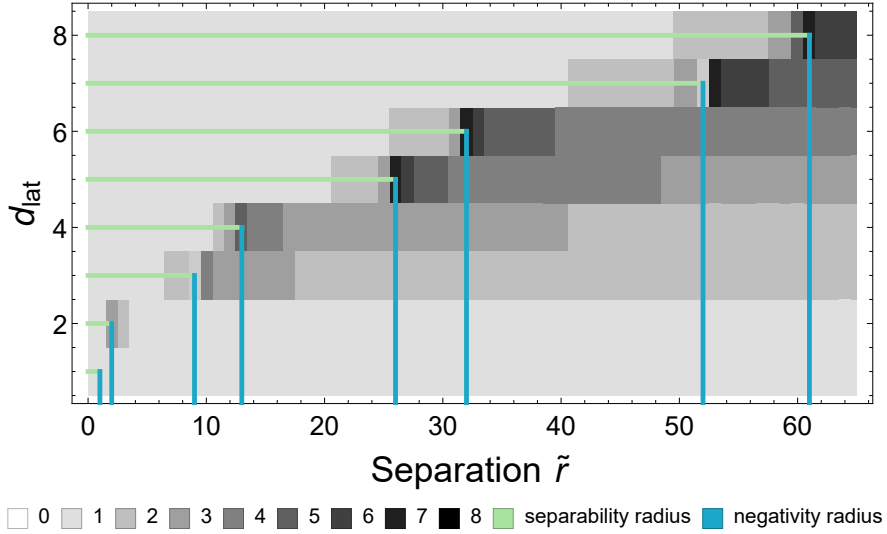


FIG. 4. (Upper panel) Steps in the covariance matrix flow arising from two regions of 1D lattice scalar field theory vacuum with $d_{\text{lat}} = 6$ for a representative separation with $\tilde{r} = 34$ outside the separability sphere, as defined in Eq. (B1). (Lower panel) The separability and negativity radii are shown to coincide for a range of d_{lat} .

For the specific application to Gaussian states representing the free scalar vacuum, both vanishing and non-vanishing negativity calculations become more informative. As such, the free scalar vacuum is a special case, distinct but reminiscent of e.g., the $(1 \times N)$ -mode or bisymmetric Gaussian states for which the negativity is known to be a necessary and sufficient condition for entanglement. For Gaussian states, if a bipartite system is found to have non-zero negativity (NPT), then non-zero distillable entanglement is determined to be present [79].

To further analyze the systems beyond the negativity sphere with vanishing negativity (positive partial transpose, PPT), the entanglement criterion of Ref. [47] can be profitably employed. A “flow” for the vacuum state covariance matrix, σ , was designed of the following form

$$\sigma_0 = \begin{pmatrix} A_0 & C_0 \\ C_0^T & B_0 \end{pmatrix}, \quad \sigma_{N+1} = \begin{pmatrix} A_N - \text{Re}(X_N) & -\text{Im}(X_N) \\ -\text{Im}(X_N^T) & A_N - \text{Re}(X_N) \end{pmatrix}, \quad (\text{B1})$$

with $X_N = C_N(B_N - i\Omega)^{-1}C_N^T$ inspired by the Schur complement’s relation to the matrix positivity condition. For the N continuous variable modes of the field, $i\Omega = [\hat{\mathbf{r}}, \hat{\mathbf{r}}^T]$ is the matrix of canonical commutation relations incorporating the uncertainty principle into the symplectic language with $\hat{\mathbf{r}}$ the $2N$ dimensional vector of $\hat{\phi}_i, \hat{\pi}_i$ canonical operators. It is shown in Ref. [47] that this non-linear map preserves the separability of states, flowing (in)separable states to (in)separable states. In addition to this preservation, the flow is demonstrated to transform covariance matrices into forms for which the separability criterion can be more readily determined by calculating e.g., the physicality of the reduced covariance matrix of the first region, A_N , indicating inseparability if A_N fails to pass the uncertainty principle requirements of $\sigma_{\text{phys}} - i\Omega \geq 0$. While the two criteria used to “detect” separability or inseparability of σ are commonly inconclusive when applied to covariance matrices, a few steps of the separability-preserving flow in

practice produce a σ_N whose separability condition can be conclusively determined, and thus that of σ_0 determined by extension.

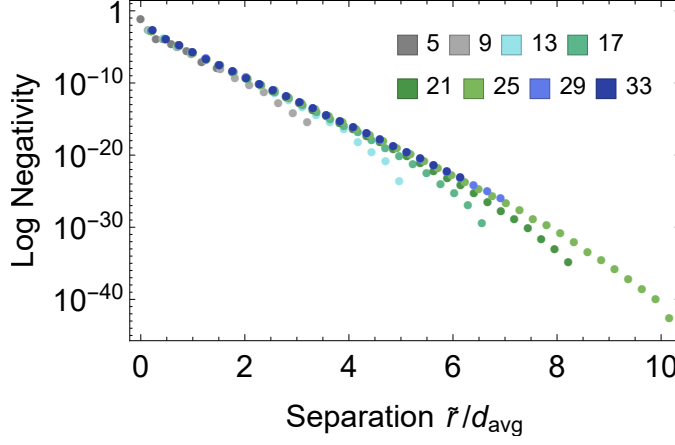
For example, consider the case of 6-site field regions ($d_{\text{lat}} = 6$) in 1D of the massless non-interacting lattice scalar field. As previously calculated (e.g., Ref. [52]) the first lattice separation at which the negativity vanishes for this system, defining the negativity radius, is $\tilde{r}_{\mathcal{N}} = 32$. Inside this radius, the non-zero negativity indicates inseparability, but at and outside this separation, the vanishing negativity does not inform the separability of the field regions. Employing the separability-preserving non-linear map [47] in Eq. (B1) for a representative separation outside the negativity sphere of $\tilde{r} = 34$ produces the covariance matrix flow shown at the top of Fig. 4. The initial covariance matrix at flow step 0, written in the basis $\hat{\mathbf{r}} = \{\hat{\phi}_0, \hat{\pi}_0, \hat{\phi}_1, \hat{\pi}_1, \dots, \hat{\phi}_5, \hat{\pi}_5\}$, is inconclusive with regard to the separability and inseparability criteria. However, after 5 flow steps, the covariance matrix σ_5 is determined to be separable. In this case, the flow arrives at the clearly separable fixed point in which the off-diagonal covariance matrix elements between regions vanish, though the criterion is capable of identifying separability prior to this point. The separability of σ_5 implies (by design) also the separability of σ_0 , indicating that the vanishing negativity in this example is the result of a stronger condition that the two regions of the field are separable.

Exploring further this flow and the relationship between negativity and separability in the lattice scalar field ground state, the lower panel of Fig. 4 shows a gray-scale distribution of the number of flow steps necessary to conclusively determine separability. It can be clearly seen that the number of flow steps necessary to determine separability/inseparability is maximized along the surface of the negativity sphere. Unfortunately, the correlation matrices explored throughout the flow evolution become poorly conditioned at increased pixelations, requiring careful control of numerical precision even far from the continuum. Furthermore, Fig. 4 shows that the negativity radii (vertical blue lines), as calculated from Ref. [52] for each d_{lat} indicated by the line's height, exactly agree with the separability radii (length of horizontal green lines), determined by flowing each covariance matrix of region diameter d_{lat} and lattice region separation \tilde{r} . As discussed in the main text, this comparison indicates that the free lattice scalar field theory vacuum is a non-generic quantum state for which vanishing negativity is coincident with separability. The resulting promotion of the *negativity sphere* to an *entanglement sphere* emphasizes that negativity serves, in this case, as a clear quantifier of experimentally relevant quantum correlations. Spacelike separated detectors interacting locally with the vacuum at regions carrying zero/non-zero negativity will never/always be able to extract, in principle, entanglement from the vacuum.

Appendix C: Numerical Calculation of β_{3D} and γ_{3D}

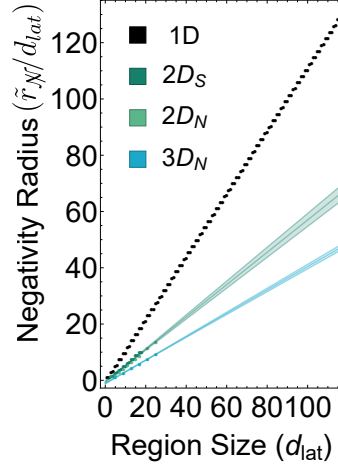
In this appendix we elaborate on our calculation of the negativity between two pixelated spherical regions of massless noninteracting lattice scalar field theory in 3D, in particular the values of $\beta_{3D} = 7.6(1)$ and $\gamma_{3D} = 0.43(2)$, which are first calculations of these quantities. In general, the calculation follows the same procedure that led to the determinations of $\beta_{1D,2D}$ and $\gamma_{1D,2D}$ presented in previous works, but there are slight differences. The geometry of the calculation is that of two equal sized, approximately spherical pixelated regions of the lattice defining the two regions, A and B , that are separated along one of the Cartesian directions. Each region has a diameter along an axis defined by d_{lat} lattice sites and of length $(d_{\text{lat}} - 1)a$, and are separated by a surface-to-surface distance of $(\tilde{r} + 1)a$ and a distance between centers of $ra = (\tilde{r} + d_{\text{lat}} - 1)a$ lattice sites. (d_{lat} even or odd are both legitimate choices at finite lattice spacing that will produce the same continuum limit.)

Transverse dimensions are distinguished from the displacement direction. While calculations of negativity can proceed by the computation of two-point correlation functions followed by direct matrix diagonalization, the dimensionality of the problem in higher dimensions and the condition number of the matrix (from the polynomial scaling correlators giving rise to an exponentially decreasing negativity), motivate utilizing the discrete symmetries of the system from the outset. These include parity, reflections in the displacement plane and hypercubic symmetries. Due to their observed dominant contribution to the negativity, we form the A_1^+ irreps of the transverse $H(D-1)$ group, defined by their radius from the transverse symmetry axis (including multiplicities where appropriate) for each distance along the displacement axis. These coordinates are used to construct the \hat{G} and \hat{H} matrices. For a given configuration, the



$1/d_{\text{lat}}$	$\beta_{3D}(d)$
0.030	7.6901(89)
0.034	7.735(15)
0.040	7.732(15)
0.048	8.014(65)
0.059	8.38(11)
0.077	9.70(16)
0.111	10.01(19)

FIG. 5. (Left) The calculated log negativity for different pixelations of 3D spheres. The values are provided in Table I. (Right) The values of $\beta_{3D}^{(\text{eff})}$ determined for each pixelation, with the extrapolation to $1/d \rightarrow 0$ defining the continuum limit.



d_{lat}	$\tilde{r}_{\mathcal{N}}/d_{\text{avg}}$	$\tilde{r}_{\mathcal{N}}/d_{\text{lat}}$
5	1.46	1.0
9	3.20(+0.14)	2.56(+0.11)
13	4.97(+0.18)	4.31(+0.15)
17	6.55(+0.2)	5.83(+0.18)
21	8.21(+0.21)	7.57(+0.19)
25	10.16(+0.22)	9.32(+0.2)

FIG. 6. (Left) The log negativity radius as a function of pixelation in 1D, 2D and 3D. The slopes provide $\gamma_{1D,2D,3D}$. The results shown for 1D and 2D are those from Ref. [52]. (Right) Numerical locations of the last calculated non-zero negativity at the entanglement sphere. The uncertainties express the inexact determination of $\tilde{r}_{\mathcal{N}}$ with the chosen separation sample density.

calculation proceeds as follows:

1. define the lattice sites in regions A and B ,
2. determine the displacement vectors for each pair of A_1^+ in the system for a given longitudinal displacement,
3. numerically evaluate the integrals $G(\mathbf{n})$ and $H^\Gamma(\mathbf{n})$ (in the text) or retrieve the stored values, and form the appropriate symmetry combination,
4. multiply \hat{G} and \hat{H}^Γ , and find the negative eigenvalues.

The calculations that we present here were performed using a combination of **Mathematica** and **Matlab**, due to their different optimizations for the combinations of analytic and numeric functions we have employed. In order to move beyond the calculations we show, more robust and scalable codes optimized for large-scale parallel computing will be required. The results of our calculations in 3D are provided in Table I and displayed in Fig. 5.

Leveraging techniques widely-used in the analysis of lattice QCD calculations, an effective mass is generated for each point in each of the sets of results given in Table I. The effective masses tend to a constant from both small and large displacements, with a range that increases and oscillatory contributions that diminish with denser pixelation of the

spheres. These effective masses lend themselves to Fourier transformation to extract the asymptotic constant with an associated uncertainty (the argument of the purely exponential behavior of the negativity) for each level of pixelation. The results of this extraction are presented in the table at the right of Fig. 5. For coarse pixelation, the range of non-vanishing negativity that we have computed is sufficiently limited that a robust estimate of the systematic errors are not practical, and we have been able to compute only three reliable values of the argument of the exponential that can be used to extrapolate to the continuum with confidence. A linear extrapolation of the three results in Fig. 5 with the smallest values of $1/d$ yields $\beta_{3D} = 7.6(1)$. A higher precision result will require additional calculations at finer pixelation, which will enable extrapolations using higher-order polynomials. The present calculations, unlike our results in 2D, are the minimum that can be performed to obtain an extrapolated value.

The values of the points of vanishing negativity as a function of pixelation determine the coefficient γ_{3D} . The results shown in Table I of the negativity as a function of separation furnish the results given in the table at the right of Fig. 6 for the (dimensionless) point of vanishing negativity. Extracting the slope of these results with respect to d_{lat} yields a value of $\gamma_{3D} = 0.43(2)$. It is interesting that the suppression of fluctuations in higher dimension has allowed the precision attained in 3D to be commensurate with that attained in 2D. These numerical calculations provide early insight into the dependence of the vacuum entanglement structure on the spatial dimension of the field, yielding results sufficiently intriguing to motivate future calculations with higher precision and in higher dimension.

Appendix D: Dispersion Relation Improvement in One Dimension

The numerical lattice scalar field theory calculations performed in this work, and the results of previously published works (e.g., Refs. [17, 52]), have employed the simplest discretization of the lattice energy-momentum relation in which the continuum momentum operator is approximated by a nearest neighbor finite-difference operation on lattice sites. It is helpful to quantify the sensitivity of the physics results we have presented in this paper to the choice of lattice discretization of this gradient operator. It is well known how to systematically improve the dispersion relation by introducing higher order operators, suppressed by positive powers of the lattice spacing, to remove higher-order contributions in momentum and to converge toward the desired $E^2 = k^2 + m^2$ of special relativity. However, for a finite number of lattice sites, only a finite number of independent finite-difference operators may be constructed, and each order of improvement corresponds to further smearing of the gradient operator over an increasing region of the lattice. To explore the impact of the discretization, we compare results in one dimension obtained with lattice dispersion relations of the form:

$$\begin{aligned} m^2 + 4 \sin^2(k/2) &\rightarrow m^2 + k^2 - \frac{k^4}{12} + \frac{k^6}{360} - \frac{k^8}{20160} + \mathcal{O}(k^{10}) \\ m^2 + 4 \sin^2(k/2) + \frac{4}{3} \sin^4(k/2) &\rightarrow m^2 + k^2 - \frac{k^6}{90} + \frac{k^8}{1008} + \mathcal{O}(k^{10}) \quad , \end{aligned} \quad (\text{D1})$$

which have the same low-momentum behavior up to polynomial corrections and differ by $\mathcal{O}(1)$ at the edge of the Brillouin zone. These correspond to different discretizations while preserving the infrared behavior of the lattice scalar field theory, and correspond to leading order and $\mathcal{O}(k^4)$ -improved lattice actions for the non-interacting lattice theory. While it might be tempting to consider the full dispersion relation directly, with the finite number of lattice sites in the system such an operator cannot be accurately obtained from a finite number of finite-difference operators. Different discretizations of the scalar field that preserve the energy-momentum relation correspond to including smearings of the gradient operator, and can be included as higher-order terms in the dispersion relation. As the goal of this Appendix is to illustrate the impact of modified UV physics on the entanglement structure of the field and because modified lattice actions are closely related to smearing for bosonic fields, the first order improvement of the dispersion relation is chosen to favor the relative impact of the UV modification.

In this Appendix, the negativity between two vacuum regions is calculated through two-point functions in which the naïve lattice dispersion relations (see Appendix A), are replaced by the k^4 -improved relations in Eq. (D1). Numerical evaluations of the correlation functions become increasingly weighted to low momentum at large distances, with the higher-order improvements making a decreasing contribution to each of the integrals. On the other hand, the

\bar{r}/d_{avg}	\mathcal{N}
$d_{\text{lat}} = 17$	
1.99×10^{-1}	2.32×10^{-3}
4.63×10^{-1}	1.83×10^{-4}
7.28×10^{-1}	1.97×10^{-5}
9.93×10^{-1}	2.34×10^{-6}
1.26	2.68×10^{-7}
1.52	3.97×10^{-8}
1.79	4.18×10^{-9}
2.05	4.68×10^{-10}
2.32	7.23×10^{-11}
2.58	8.65×10^{-12}
2.85	1.01×10^{-12}
3.11	1.28×10^{-13}
3.38	1.52×10^{-14}
3.64	1.43×10^{-15}
3.91	1.58×10^{-16}
4.17	2.09×10^{-17}
4.44	1.65×10^{-18}
4.7	1.55×10^{-19}
4.97	9.53×10^{-21}
5.23	7.83×10^{-22}
5.5	4.67×10^{-23}
5.76	1.60×10^{-24}
6.03	7.07×10^{-26}
6.29	1.84×10^{-27}
6.55	6.29×10^{-30}
$d_{\text{lat}} = 21$	
2.07×10^{-1}	2.64×10^{-3}
4.65×10^{-1}	1.84×10^{-4}
7.23×10^{-1}	2.24×10^{-5}
9.81×10^{-1}	2.45×10^{-6}
1.24	3.30×10^{-7}
1.5	4.42×10^{-8}
1.76	4.79×10^{-9}
2.01	7.28×10^{-10}
2.27	9.43×10^{-11}
2.53	1.16×10^{-11}
2.79	1.83×10^{-12}
3.05	2.27×10^{-13}
3.31	2.49×10^{-14}
3.56	3.53×10^{-15}
3.82	4.55×10^{-16}
4.08	5.46×10^{-17}
4.34	6.83×10^{-18}
4.6	8.56×10^{-19}
4.86	9.23×10^{-20}
5.11	9.97×10^{-21}
5.37	9.97×10^{-22}
5.63	9.76×10^{-23}
5.89	8.84×10^{-24}
6.15	9.80×10^{-25}
6.41	7.34×10^{-26}
6.66	4.72×10^{-27}
6.92	2.69×10^{-28}
7.18	2.05×10^{-29}
7.44	1.02×10^{-30}
7.7	3.04×10^{-32}
7.96	1.37×10^{-33}
8.21	2.41×10^{-35}

\bar{r}/d_{avg}	\mathcal{N}
$d_{\text{lat}} = 25$	
2.18×10^{-1}	2.63×10^{-3}
4.79×10^{-1}	1.76×10^{-4}
7.41×10^{-1}	2.22×10^{-5}
1.	2.34×10^{-6}
1.26	3.34×10^{-7}
1.53	3.89×10^{-8}
1.79	5.17×10^{-9}
2.05	7.45×10^{-10}
2.31	8.57×10^{-11}
2.57	1.31×10^{-11}
2.83	1.83×10^{-12}
3.09	2.17×10^{-13}
3.36	3.20×10^{-14}
3.62	4.42×10^{-15}
3.88	5.13×10^{-16}
4.14	6.94×10^{-17}
4.4	9.14×10^{-18}
4.66	1.22×10^{-18}
4.93	1.47×10^{-19}
5.19	1.82×10^{-20}
5.45	2.03×10^{-21}
5.71	2.23×10^{-22}
5.97	2.60×10^{-23}
6.23	2.66×10^{-24}
6.49	2.93×10^{-25}
6.76	3.07×10^{-26}
7.02	2.89×10^{-27}
7.28	3.09×10^{-28}
7.54	2.26×10^{-29}
7.8	2.71×10^{-30}
8.06	2.19×10^{-31}
8.32	1.17×10^{-32}
8.59	6.11×10^{-34}
8.85	3.84×10^{-35}
9.11	2.11×10^{-36}
9.37	9.88×10^{-38}
9.63	4.29×10^{-39}
9.89	1.54×10^{-40}
1.02×10^1	3.35×10^{-43}

\bar{r}/d_{avg}	\mathcal{N}
$d_{\text{lat}} = 29$	
2.21×10^{-1}	2.80×10^{-3}
4.78×10^{-1}	1.92×10^{-4}
7.36×10^{-1}	2.34×10^{-5}
9.93×10^{-1}	2.60×10^{-6}
1.25	3.67×10^{-7}
1.51	4.23×10^{-8}
1.77	6.29×10^{-9}
2.02	8.45×10^{-10}
2.28	1.08×10^{-10}
2.54	1.67×10^{-11}
2.8	2.20×10^{-12}
3.05	3.02×10^{-13}
3.31	4.44×10^{-14}
3.57	5.79×10^{-15}
3.83	7.79×10^{-16}
4.08	1.10×10^{-16}
4.34	1.42×10^{-17}
4.6	1.93×10^{-18}
4.86	2.62×10^{-19}
5.11	3.32×10^{-20}
5.37	4.36×10^{-21}
5.63	5.82×10^{-22}
5.89	7.26×10^{-23}
6.14	9.13×10^{-24}
6.4	1.20×10^{-24}
6.66	1.50×10^{-25}
6.92	1.60×10^{-26}
$d_{\text{lat}} = 33$	
2.25×10^{-1}	2.71×10^{-3}
4.82×10^{-1}	1.90×10^{-4}
7.39×10^{-1}	2.24×10^{-5}
9.97×10^{-1}	2.58×10^{-6}
1.25	3.47×10^{-7}
1.51	4.20×10^{-8}
1.77	6.28×10^{-9}
2.03	7.75×10^{-10}
2.28	1.10×10^{-10}
2.54	1.61×10^{-11}
2.8	2.08×10^{-12}
3.05	3.17×10^{-13}
3.31	4.37×10^{-14}
3.57	5.71×10^{-15}
3.83	8.27×10^{-16}
4.08	1.13×10^{-16}
4.34	1.53×10^{-17}
4.6	2.15×10^{-18}
4.85	2.87×10^{-19}
5.11	3.92×10^{-20}
5.37	5.28×10^{-21}
5.63	6.77×10^{-22}
5.88	8.52×10^{-23}
6.14	1.13×10^{-23}

TABLE I. The numerically determined negativity between 3D pixelated spherical lattice regions as a function of normalized separation. The columns of finer-pixelation ($d = 29, 33$) do not show results throughout the entire range of non-vanishing negativity.

long-distance negativity becomes increasingly sensitive to the short-distance behavior of the two-point functions and does explicitly probe these higher-order improvements, consistent with the main thesis of this article. Together, these observations indicate the presence of large cancelations between polynomially- and logarithmically-varying correlation functions at long distances to produce an exponentially decaying residual sensitive to the short-distance physics. Table II shows the results obtained for the radius of the negativity sphere for different region sizes using the improved lattice dispersion relations. The negativity between regions of different sizes are shown in Fig. 7 for two different dispersion relations. Away from the continuum limit, the negativity exhibits oscillations that depend upon the dispersion relation, and as such lead to fluctuations in the separability radius but do not change the scale setting the exponential dependence on separation. As discussed, the negativity at smaller separations is less sensitive to the high-momentum behavior, consistent with a smaller dependence on the dispersion relation improvement.

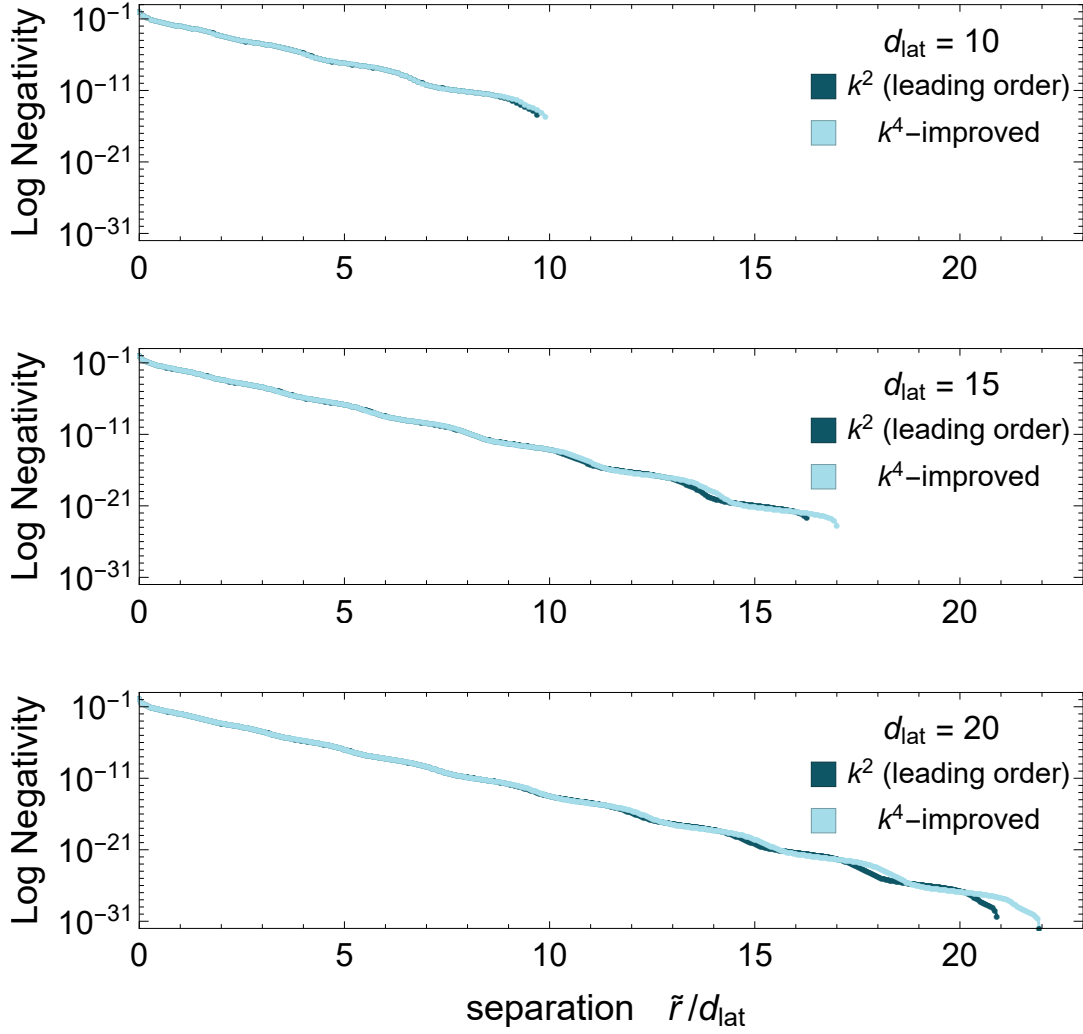


FIG. 7. The logarithmic negativity calculated with two different dispersion relations (k^2 leading order and k^4 -improved) for one-dimensional region lengths of 10(top), 15(middle), and 20(bottom) lattice sites. Sensitivity to the UV modification appears at large spatial separation, as discussed in the main text.

k^2					k^4						
d_{lat}	$\tilde{r}_{\mathcal{N}}$	$\tilde{r}_{\mathcal{N}}/d_{lat}$			d_{lat}	$\tilde{r}_{\mathcal{N}}$	$\tilde{r}_{\mathcal{N}}/d_{lat}$				
1	1	1.00	11	131	11.90	1	1	1.00	11	135	12.30
2	2	1.00	12	144	12.00	2	2	1.00	12	148	12.30
3	9	3.00	13	184	14.20	3	9	3.00	13	190	14.60
4	13	3.25	14	199	14.20	4	12	3.00	14	207	14.80
5	26	5.20	15	245	16.30	5	26	5.20	15	256	17.10
6	32	5.33	16	264	16.50	6	32	5.33	16	275	17.20
7	52	7.43	17	316	18.60	7	53	7.57	17	331	19.50
8	61	7.63	18	337	18.70	8	61	7.63	18	352	19.60
9	87	9.67	19	395	20.80	9	89	9.89	19	415	21.80
10	98	9.80	20	419	21.00	10	100	10.00	20	440	22.00

TABLE II. Negativity sphere radii for regions of the one-dimensional massless scalar field with a nearest neighbor lattice action (k^2) and order k^4 -improvement of the dispersion relation.